Journal of Alloys and Compounds 509 (2011) 1554–1562

Contents lists available at ScienceDirect

Journal of Alloys and Compounds

journal homepage: www.elsevier.com/locate/jallcom

Experimental investigation and thermodynamic calculation of the phase equilibria in the Co–Nb–Ta ternary system

L. Zhou[a], C.P. Wang[a], Y. Yu[a], X.J. Liu[a,*], H. Chinen[b], T. Omori[b], I. Ohnuma[b], R. Kainuma[b], K. Ishida[b]

[a] Department of Materials Science and Engineering, College of Materials, and Research Center of Materials Design and Applications, Xiamen University, Xiamen, 361005, P.R. China
[b] Department of Materials Science, Graduate School of Engineering, Tohoku University, Aoba-yama 6-6-02, Sendai 980-8579, Japan

ARTICLE INFO

Article history:
Received 21 September 2010
Received in revised form 8 October 2010
Accepted 8 October 2010
Available online 21 October 2010

Keywords:
Metals and alloys
Phase diagrams
X-ray diffraction

ABSTRACT

The isothermal sections of the Co–Nb–Ta ternary system at 900 °C, 1000 °C, 1100 °C, 1200 °C, 1300 °C have been experimentally determined by electron probe microanalysis (EPMA) and X-ray diffraction (XRD) techniques on the equilibrated alloys. On the basis of the experimental data investigated in the present work, the phase equilibria in the Co–Nb–Ta system has been thermodynamically assessed by using CALPHAD (CALculation of PHAse Diagrams) method, and a consistent set of the thermodynamic parameters leading to reasonable agreement between the calculated results and experimental data was obtained.

1. Introduction

The Co-based alloys are important industrial materials in applications of wear-resistant coatings, magnetic materials and high-temperature alloys [1,2]. Recently, great attention has been paid to the newly discovered γ′ phase ($L1_2$ structure) strengthening Co–Al–W high-temperature alloy [3], which shows the same strengthening mechanism as the commonly used Ni-based heat resistant alloy strengthened by the γ′ phase (Ni_3Al, $L1_2$ structure). Thus, the Co–Al–W high-temperature alloys show potential application in the field of aircraft turbines and combustor sections due to their superior stress–rupture parameters, excellent hot corrosion, good oxidation resistance and thermal fatigue resistance etc. [4,5]. In order to further improve the stability of the γ′ phase in the Co–Al–W alloys, the γ′ phase stabilizing elements, such as Nb, Ta, Mo, Ti and V, were usually added [6]. Therefore, for the purpose of improving the properties of the high-temperature alloys and understanding the relationship between microstructure and properties, accurate knowledge of the phase equilibria in the multi-component Co–Al–W–Mo–Nb–Ta–Ti–V system is of great essence.

Recently, the present authors have focused on developing a thermodynamic database of the phase diagrams in the Co–Al–W–Mo–Nb–Ta–Ti–V system [3,7–14], and the Co–Nb–Ta system is one of the important subsystems. Thus, the information on phase equilibria in the Co–Nb–Ta system is required. However, only an isothermal section at 1100 °C in the Co–Nb–Ta system experimentally investigated and thermodynamically predicted by Ishchenko [15] was reported. Therefore, it is important and necessary to comprehensively determine the phase equilibria in the Co–Nb–Ta ternary system. Obtaining such information exclusively from experiments is burdensome and expensive. The CALPHAD (CALculation of PHAse Diagrams) technique, which has been recognized to be an important tool to significantly reduce time and cost during the development of materials, can effectively provide a clear guidance for the materials design [16–18]. As a part of the thermodynamic database of phase diagrams in multi-component Co–Al–W–Mo–Nb–Ta–Ti–V system, the thermodynamic description for the Co–Nb–Ta ternary system supported by key experiments is of great essence.

The objective of the present work is to experimentally investigate the phase equilibria in the Co–Nb–Ta ternary system, and to carry out the thermodynamic assessment of the Co–Nb–Ta ternary system on the basis of the experimental data and the assessed sub-binary systems.

2. Experimental procedure

Bulk Co–Nb–Ta alloy buttons were prepared from high-purity Co (99.9 wt.%), Nb (99.9 wt.%), and Ta (99.9 wt.%) by arc melting under an argon atmosphere using a non-consumable tungsten electrode. The ingots were melted at least six times in order to achieve their homogeneity. The sample weight was around 15 g and the weight loss during melting was generally less than 0.20% of the sample weight. Afterwards, the ingots were cut into small pieces for heat treatments and further observations.

* Corresponding author at: Department of Materials Science and Engineering, College of Materials, Xiamen University, Xiamen 361005, PR China.
E-mail address: lxj@xmu.edu.cn (X.J. Liu).

0925-8388/$ – see front matter © 2010 Elsevier B.V. All rights reserved.
doi:10.1016/j.jallcom.2010.10.058

Table 1
The structures and the used models of phases in the Co–Nb–Ta ternary system.

Phase	Pearson's symbol	Prototype	Structure type	Thermodynamic model	Used model
bcc	*cI2*	W	A2	(Co, Nb, Ta)	SSM
CoM_2	*tI12*	Al_2Cu	C16	$(Co)_1(Nb, Ta)_2$	SM
μ (Co_7M_6)	*hR13*	Fe_7W_6	D85	$(Co,Nb,Ta)_1(Co,Nb,Ta)_2(Co)_6(Nb,Ta)_4$	SM
$Co_{16}M_9$	*hp12*	$MgZn_2$	C14	$(Co)_{16}(Nb, Ta)_9$	SM
λ (Co_2M)	*cF24*	Cu_2Mg	C15	$(Co, Nb, Ta)_2(Co, Nb, Ta)_1$	SM
Co_3M	*hP24*	$MgNi_2$	C36	$(Co)_3(Nb, Ta)_1$	SM
Co_7M_2	–	–	–	$(Co)_7(Nb, Ta)_2$	SM
Liquid	–	–	–	(Co, Nb, Ta)	SSM
αCo	*cF4*	Cu	A1	(Co, Nb, Ta)	SSM
εCo	*hP2*	Mg	A3	(Co, Nb, Ta)	SSM

Note: SSM: subregular solution model; SM: sublattice model.

Plate-shaped specimens were wrapped in Mo foil in order to prevent direct contact with the quartz ampoule, and put in quartz capsule evacuated and backfilled with argon gas. The specimens were annealed at 1300 °C, 1200 °C, 1100 °C, 1000 °C and 900 °C, respectively. The time of the heat treatment varied from several hours and several weeks depending on the annealing temperature and the composition of the specimen. After the heat treatment, the specimens were quenched into ice water.

After standard metallographic preparation, the microstructural observations were carried out by optical microscopy (OM). The equilibrium compositions of the equilibrated alloys were examined by electron probe microanalysis (EPMA) (JXA-8100R, JEOL, Japan). Pure elements were used as standards and the measurements were carried out at 20.0 kV. The X-ray diffraction (XRD) was used to identify the crystal structure of the constituent phases. The XRD measurement was carried out on a Phillips Panalytical X-pert diffractometer using CuKα radiation at 40 kV and 30 mA. The data were collected in the ranges of 2θ from 30° to 90° at a step width of 0.0167°.

3. Thermodynamic models

The thermodynamic assessment of the Co–Nb–Ta ternary system was carried out by the CALPHAD method, and the structures and the used models of all phases in the Co–Nb–Ta ternary system are listed in Table 1.

3.1. Solution phases

The Gibbs free energies of the liquid, fcc, bcc, and hcp phases in the Co–Nb–Ta system are described by the subregular solution model. According to this model, the Gibbs free energy of ϕ phase in the Co–Nb–Ta system is expressed by:

$$G_m^\phi = \sum_{i=Co,Nb,Ta} x_i^0 G_i^\phi + RT \sum_{i=Co,Nb,Ta} x_i \ln x_i^\phi + {}^{ex}G^\phi + {}^{mg}G^\phi i\phi, \quad (1)$$

where G_i^ϕ is the molar Gibbs free energy of pure element i in the structure ϕ phase, and the term ${}^{ex}G^\phi$ is the excess free energy, which is expressed by the Redlich–Kister polynomials [19] as:

$${}^{ex}G^\phi = x_{Co}x_{Nb}L^\phi_{Co,Nb} + x_{Co}x_{Ta}L^\phi_{Co,Ta} + x_{Nb}x_{Ta}L^\phi_{Nb,Ta} + x_{Co}x_{Nb}x_{Ta}L^\phi_{Co,Nb,Ta}, \quad (2)$$

$$L^\phi_{i,j} = \sum_{m=0}^{n} {}^mL^\phi_{i,j}(x_i - x_j)^m, \quad (3)$$

$$L^\phi_{Co,Nb,Ta} = x_{Co}{}^0L^\phi_{Co,Nb,Ta} + x_{Nb}{}^1L^\phi_{Co,Nb,Ta} + x_{Ta}{}^2L^\phi_{Co,Nb,Ta}, \quad (4)$$

where $L^\phi_{i,j}$ is the interaction parameter in the i − j binary system, and the ternary interaction coefficient $L^\phi_{Co,Nb,Ta}$ is assumed to be zero in the present work.

In the Co–Nb–Ta ternary system, there is a ferromagnetic orderingcontribution to Gibbs free energy for the fcc, bcc and hcp phases due to the presence of cobalt. The term ${}^{mg}G^\phi$ is expressed as follows [17]:

$${}^{mg}G^\phi = RT\ \ln(\beta^\phi + 1)f(\tau^\phi) \quad \tau^\phi = \frac{T}{T_c^\phi}, \quad (5)$$

where β^ϕ is the quantity related to the total magnetic entropy, which in most cases is set to Bohr magnetic moment per mole of atoms; $f(\tau^\phi)$ is the polynomial function of τ, and T_c^ϕ is the critical temperature for magnetic ordering, T_c^ϕ and β^ϕ are described by the following expressions:

$$T_c^\phi = \sum_i x_i T_i^\phi + x_i x_j \sum_{m=0}^{n} {}^mT^\phi_{i,j}(x_i - x_j)^m, \quad (6)$$

$$(i, j = Co, Nb \text{ or } Ta \quad \text{and} \quad i \neq j), \quad (7)$$

where T_i^ϕ is the Curie temperature of pure component, and ${}^mT^\phi_{i,j}$ is the interaction term between the elements i and j (i,j = Co, Nb or Ta and i ≠ j). β_i^ϕ is the Bohr magnetic moment for pure component, ${}^m\beta^\phi_{i,j}$ is the interaction term between the elements i and j (i,j = Co, Nb or Ta and i ≠ j), and $f(\tau^\phi)$ represents the polynomials obtained by Hillert and Jarl [20] as follows:

$$f(\tau) = 1 - \frac{1}{D}\left[\frac{79\tau^{-1}}{140p} + \frac{474}{497}\left(\frac{1}{p} - 1\right)\left(\frac{\tau^3}{6} + \frac{\tau^9}{135} + \frac{\tau^{15}}{600}\right)\right] \quad \text{for} \quad t = 1, \quad (8)$$

$$f(\tau) = -\frac{1}{D}\left(\frac{\tau^{-5}}{10} + \frac{\tau^{-15}}{315} + \frac{\tau^{-25}}{1500}\right) \quad \text{for} \quad t > 1, \quad (9)$$

where $D = (518/1125) + (11{,}692 + 15{,}975)((1/p) - 1)$ and p depends on their structure, 0.4 for the bcc structure and 0.28 for others.

3.2. The intermetallic compound Co_aM_b

In the literature [15,21], the intermetallic compounds Co_aM_b (Co_7M_2, Co_3M, $Co_{16}M_9$ and CoM_2 (M = Nb or Ta) were treated as line compound in Co–Ta and Co–Nb binary system. Considering the ternary solubility in the above-mentioned Co_aM_b compounds, the Co_7M_2, Co_3M, $Co_{16}M_9$ and CoM_2 phases (M = Nb, Ta) in the Co–Nb–Ta ternary system, is described by the sublattice model as $(Co)_7(Nb,Ta)_2$, $(Co)_3(Nb,Ta)_1$, $(Co)_{16}(Nb,Ta)_9$ and $(Co)_1(Nb,Ta)_2$, respectively. The molar Gibbs free energy for the $(Co)_a(Nb,Ta)_b$ compound is expressed as follows:

$$G_m^\phi = y^{II}_{Nb}G_{Co:Nb} + y^{II}_{Ta}G_{Co:Ta} + bRT(y^{II}_{Nb}\ln y^{II}_{Nb} + y^{II}_{Ta}\ln y^{II}_{Ta}) + y^{II}_{Nb}y^{II}_{Ta}\left[\sum_{m=0}^{n} {}^nL_{Co:Nb,Ta}(y^{II}_{Nb} - y^{II}_{Ta})^n\right] \quad (10)$$

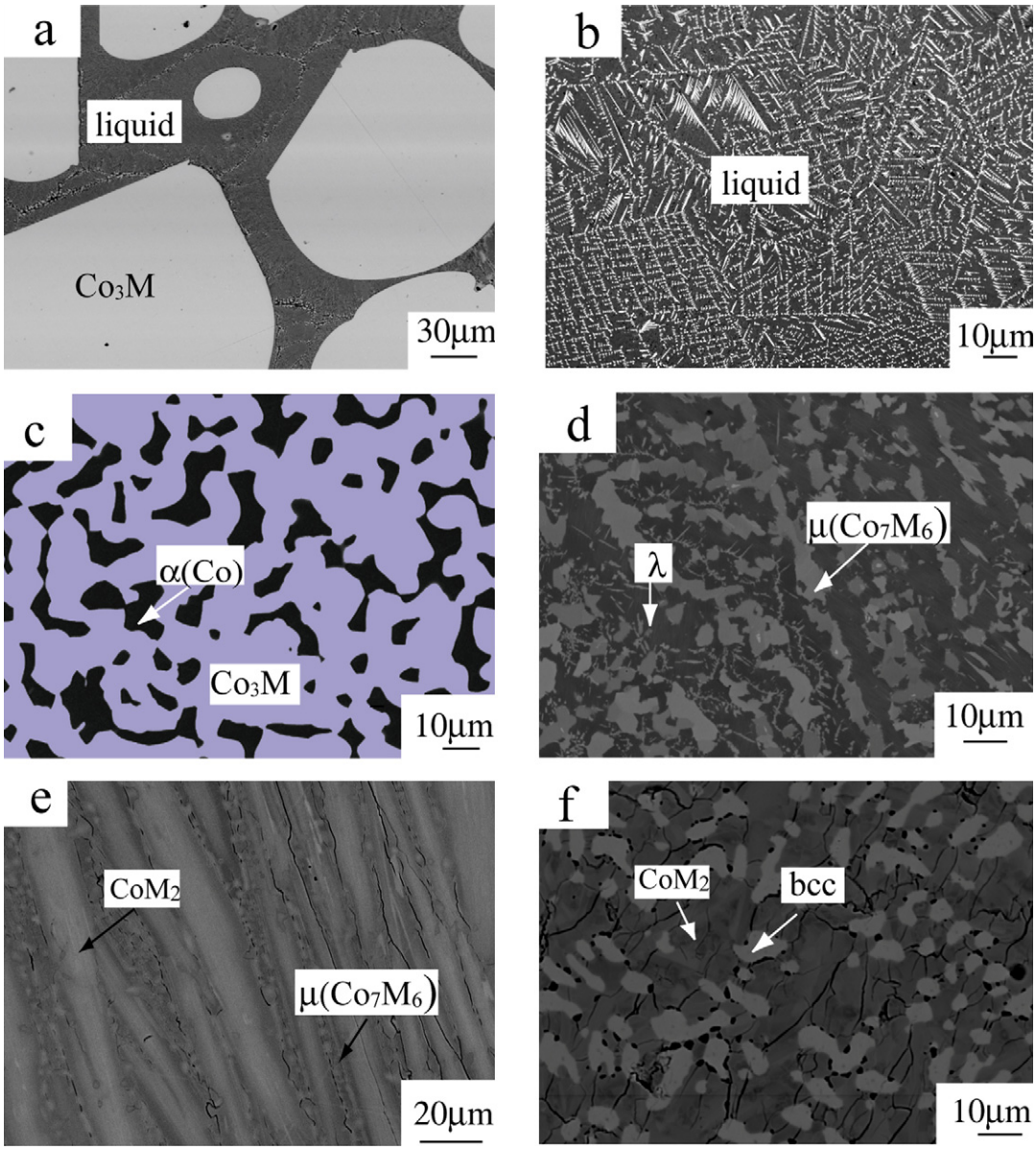

Fig. 1. BSE image of the typical Co–Nb–Ta ternary alloys: (a) the $Co_{80}Nb_5Ta_{15}$ alloy annealed at 1300 °C for 24 h, (b) the $Co_{80}Nb_{10}Ta_{10}$ alloy annealed at 1300 °C for 30 days, (c) the $Co_{80}Nb_5Ta_{15}$ alloy annealed at 1200 °C for 14 days, (d) the $Co_{60}Nb_{20}Ta_{20}$ alloy annealed at 900 °C for 80 days, (e) the $Co_{40}Nb_{40}Ta_{20}$ alloy annealed at 1200 °C for 14 days, (f) the $Co_{25}Nb_{10}Ta_{65}$ alloy annealed at 1200 °C for 21 days.

where $G_{Co:Nb}$ and $G_{Co:Ta}$ are the Gibbs free energy of the Co_aNb_b and Co_aTa_b phases. And the ${}^nL_{Co:Nb,Ta}$ corresponds to the interaction parameters in the Co–Nb–Ta ternary system, and is expressed as follows:

$${}^nL_{Co:Nb,Ta} = a + bT \tag{11}$$

where a and b were evaluated in the present work.

3.3. The λ (Co_2M) phase

The λ phase (Co_2M (M = Nb or Ta and Nb, Ta)) forms the continuous solid solutions from the Co–Ta side to the Co–Nb side in the Co–Nb–Ta ternary system. The λ phase is formulated using the sublattice model, $(Co,Nb,Ta)_2(Co,Nb,Ta)_1$. According to the model, the molar Gibbs free energy of the λ phase in the Co–Nb–Ta ternary system is expressed as follows:

$$\begin{aligned} G^{\lambda} = {} & \sum_{\substack{i \\ (i=Co,Nb,Ta;\ j=Co,Nb,Ta)}}\sum_{j} y_i^{I} y_i^{II} G_{i:j}^{\lambda} + RT\left(2\sum_{\substack{i \\ (i=Co,Nb,Ta;\ j=Co,Nb,Ta)}} y_i^{I} \ln y_i^{I} + \sum_{j} y_j^{II} \ln y_j^{II}\right) \\ & + 2\sum_{i,j}\sum_{\substack{k \\ (i,j=Co,Nb,Ta,\ \text{and}\ i\neq j;\ k=Co,Nb,Ta)}}\left[y_i^{I} y_j^{I} y_k^{II}\left(\sum {}^nL_{i,j:k}(y_i^{I} - y_j^{I})^n\right)\right] \\ & + \sum_{i}\sum_{\substack{j,k \\ (i=Co,Nb,Ta;\ j,k=Co,Nb,Ta,\ \text{and}\ j\neq k)}}\left[y_i^{I} y_j^{II} y_k^{II}\left(\sum {}^nL_{i:j,k}(y_j^{II} - y_k^{II})\right)^n\right] \end{aligned} \tag{12}$$

where $G_{i:j}^{\lambda}$ is the Gibbs free energy of the λ phase, when the first sublattice is occupied by the element i (i = Co, Nb or Ta) and the second one is occupied by the element j (j = Co, Nb or Ta). The ${}^nL_{i,j:k}$ is the interaction energy between i and j in the first sublattice when

the second one is occupied by the element k (k = Co, Nb or Ta). The ${}^{n}L_{i:j,k}$ is the interaction energy between j and k in the second sublattice when the first one is occupied by the element i (i = Co, Nb or Ta). These parameters were evaluated based on the experimental data in this work.

3.4. The μ (Co_6M_7) phase

The thermodynamic model of μ (Co_6M_7) phase is described as $(Co,Nb,Ta)_1(Co,Nb,Ta)_2(Co)_6(Nb,Ta)_4$. According to this model, the molar Gibbs free energy of the μ phase in the Co–Nb–Ta ternary system is expressed as follows:

$$
\begin{aligned}
G^{\mu} = & \sum_{\substack{i \\ (i=Co,Nb,Ta;}} \sum_{\substack{j \\ j=Co,Nb,Ta;}} \sum_{\substack{k \\ k=Nb,Ta)}} y_i^{I} y_j^{II} y_k^{IV} G^{\mu}_{i:j:Co:k} \\
& + RT \left(\sum_{\substack{i \\ (i=Co,Nb,Ta;}} y_i^{I} \ln y_i^{I} + 2 \sum_{\substack{j \\ j=Co,Nb,Ta;}} y_j^{II} \ln y_j^{II} + 4 \sum_{\substack{k \\ k=Nb,Ta)}} y_k^{IV} \ln y_k^{IV} \right) \\
& + \sum_{i,j} \sum_{k} \sum_{l} \left[y_i^{I} y_j^{I} y_k^{II} y_l^{IV} \left(\sum {}^{n}L_{i,j:k:Co:l} (y_i^{I} - y_j^{I})^{n} \right) \right]_{(i,j=Co,Nb,Ta,\ \text{and}\ j=Co,Nb,Ta;\ k=Nb,Ta)} \\
& + \sum_{i} \sum_{j,k} \sum_{l} \left[y_i^{I} y_j^{I} y_k^{II} y_l^{IV} \left(\sum {}^{n}L_{i,j:k:Co:l} (y_i^{II} - y_j^{II})^{n} \right) \right]_{(i=Co,Nb,Ta;\ j,k=Co,Nb,Ta,\ \text{and}\ j \neq k;\ l=Nb,Ta)} \\
& + \sum_{i} \sum_{j,k} \sum_{l} \left[y_i^{I} y_j^{I} y_k^{II} y_l^{IV} \left(\sum {}^{n}L_{i,j:k:Co:l} (y_i^{IV} - y_j^{IV})^{n} \right) \right]_{(i=Co,Nb,Ta;\ j=Co,Nb,Ta;\ k=Nb,Ta)} \qquad (13)
\end{aligned}
$$

where $G^{\mu}_{i:j:Co:k}$ is the Gibbs free energy of the μ phase, when the first sublattice is occupied by the element i (i = Co, Nb or Ta), the second one is occupied by the element j (j = Co, Nb or Ta), the third one is occupied by the element Co, and the fourth one is occupied by the element k (k = Nb or Ta). ${}^{n}L_{i,j:k:Co:l}$ is the interaction energy between i and j in the first sublattice when the second one occupied by the element k (k = Co, Nb or Ta), the third one is occupied by the element Co, and the fourth one is occupied by the element l (l = Nb or Ta). The ${}^{n}L_{i:j,k:Co:l}$ is the interaction energy between j and k in the second sublattice when the first one is occupied by the element i (i = Co, Nb or Ta), the third one is occupied by the element Co, and the fourth one is occupied by the element l (l = Nb or Ta). ${}^{n}L_{i:j:Co:Nb,Ta}$ is the interaction energy between Nb and Ta in the fourth sublattice when the first one is occupied by i (i = Co, Nb or Ta), the second one is occupied by the element j (j = Co, Nb or Ta), and the third one is occupied by the element Co. These parameters were evaluated based on the experiment data in this work.

4. Experimental results and discussion

BSE (back-scattered electron) images of the typical ternary Co–Nb–Ta alloys are presented in Fig. 1. Phase identification was based on the equilibrium composition as measured by EPMA and XRD analysis. Two-phase equilibrium of the liquid + Co_3M was identified in the $Co_{80}Nb_5Ta_{15}$ (at.%) alloy annealed at 1300 °C for 24 h, and shown in Fig. 1(a), where the light grey Co_3M phase irregularly distributes in the matrix of the liquid phase. In the $Co_{80}Nb_{10}Ta_{10}$ (at.%) alloy quenched from 1300 °C, especially attractive dendritic structure was observed in Fig. 1(b), which is the typical microstructure of the liquid phase, and in good agreement with the reported results [15,26]. In the $Co_{80}Nb_5Ta_{15}$ (at.%) alloy annealed at 1200 °C for 14 days, two phases namely αCo and Co_3M were identified by EPMA, as shown in Fig. 1(c), where the dark grey αCo phase is completely wrapped by the Co_3M phase.

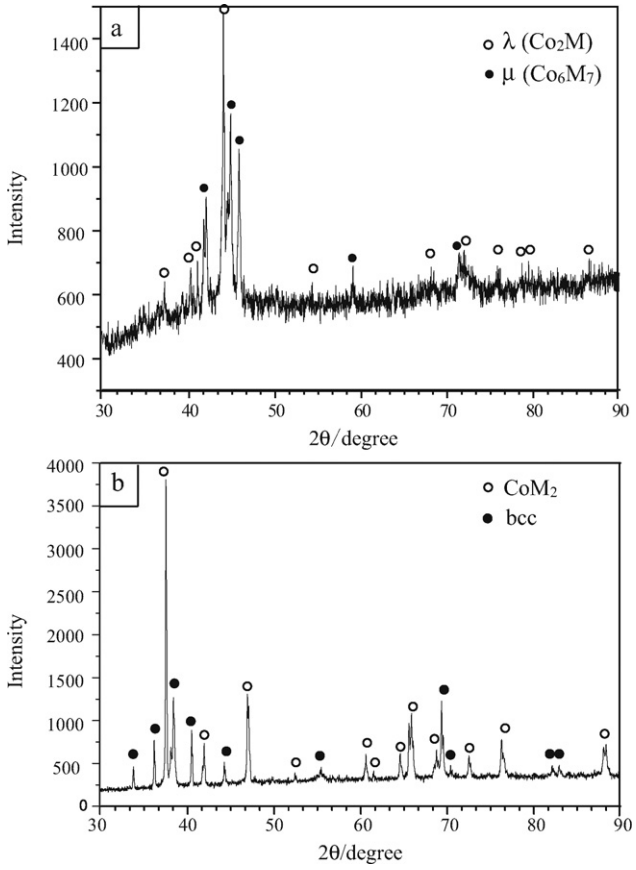

Fig. 2. X-ray diffraction patterns obtained from: (a) the $Co_{60}Nb_{30}Ta_{10}$ alloy annealed at 1100 °C for 4 weeks, and (b) the $Co_{25}Nb_{10}Ta_{65}$ alloy annealed at 1300 °C for 10 days.

The $Co_{40}Nb_{40}Ta_{20}$ (at.%) and $Co_{25}Nb_{10}Ta_{65}$ (at.%) alloy annealed at 1200 °C are located two two-phase equilibrium regions of the μ + CoM_2 and bcc + CoM_2, respectively, as characterized in Fig. 1(d) and (e). Fig. 1(f) shows the two-phase microstructure (λ + μ) of the $Co_{60}Nb_{20}Ta_{20}$ (at.%) alloy annealed at 900 °C for 80 days.

Typical X-ray diffraction patterns of the two-phase microstructures of the λ + μ and bcc + CoM_2 are presented in Fig. 2 respectively, where the characteristic peaks of different phases are well distinguished by different symbols. The equilibrium compositions of the Co–Nb–Ta ternary system at 900 °C, 1000 °C, 1100 °C, 1200 °C and 1300 °C determined by EPMA are listed in Table 2, and no ternary compound was found in this system.

The typical DSC curve for heating at 20 °C/min of the $Co_{40}Nb_{50}Ta_{10}$ (at.%) alloy is shown in Fig. 3 to present phase trans-

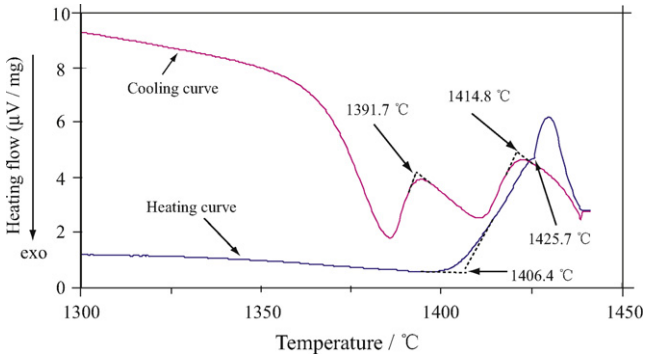

Fig. 3. Heating and cooling curves of the $Co_{40}Nb_{50}Ta_{10}$ (at.%) alloys.

Table 2
The equilibrium compositions of the Co–Nb–Ta ternary system determined in the present work.

Temp. (°C)	Alloy (at.%)	Phase equilibrium	Composition (at.%)			
			Phase 1		Phase 2	
		Phase 1/phase 2	Nb	Ta	Nb	Ta
900	$Co_{80}Nb_{10}Ta_{10}$	αCo/Co_7M_2	0.70	0.89	10.43	10.75
	$Co_{80}Nb_{15}Ta_5$	αCo/Co_7M_2	1.61	0.51	16.06	5.08
	$Co_{60}Nb_{20}Ta_{20}$	λ/μ (Co_7M_6)	16.48	17.65	23.65	22.74
	$Co_{60}Nb_{30}Ta_{10}$	λ/μ (Co_7M_6)	26.02	9.08	37.81	11.12
	$Co_{60}Nb_{35}Ta_5$	λ/μ (Co_7M_6)	30.57	4.38	41.58	5.49
	$Co_{40}Nb_{20}Ta_{40}$	μ (Co_7M_6)/CoM_2	16.61	38.58	17.71	46.23
	$Co_{40}Nb_{50}Ta_{10}$	μ (Co_7M_6)/bcc	44.56	9.88	86.23	10.30
	$Co_{25}Nb_{65}Ta_{10}$	μ (Co_7M_6)/bcc	45.18	8.79	86.29	9.33
	$Co_{25}Nb_{70}Ta_5$	μ (Co_7M_6)/bcc	49.94	4.86	92.08	4.50
	$Co_{25}Nb_{55}Ta_{20}$	CoM_2/bcc	43.83	23.70	74.46	21.82
	$Co_{25}Nb_{20}Ta_{55}$	CoM_2/bcc	13.66	51.52	25.87	69.05
	$Co_{25}Nb_{50}Ta_{25}$	CoM_2/bcc	33.80	31.47	66.85	30.20
1000	$Co_{80}Nb_{15}Ta_5$	αCo/Co_7M_2	1.21	0.48	16.38	5.21
	$Co_{80}Nb_{10}Ta_{10}$	αCo/Co_7M_2	0.60	0.81	10.27	10.43
	$Co_{60}Nb_{25}Ta_{15}$	λ/μ (Co_7M_6)	21.91	10.59	35.87	12.54
	$Co_{60}Nb_{35}Ta_5$	λ/μ (Co_7M_6)	28.22	4.30	43.12	5.33
	$Co_{60}Nb_{20}Ta_{20}$	λ/μ (Co_7M_6)	15.13	16.82	25.60	21.94
	$Co_{40}Nb_{20}Ta_{40}$	μ (Co_7M_6)/CoM_2	17.15	38.19	18.51	44.74
	$Co_{40}Nb_{40}Ta_{20}$	μ (Co_7M_6)/CoM_2	34.87	19.48	42.23	21.80
	$Co_{40}Nb_{50}Ta_{10}$	μ (Co_7M_6)/bcc	44.40	9.78	86.23	9.53
	$Co_{25}Nb_{70}Ta_5$	μ (Co_7M_6)/bcc	36.75	18.64	76.11	20.88
	$Co_{25}Nb_{55}Ta_{20}$	CoM_2/bcc	41.50	23.66	76.46	21.40
	$Co_{25}Nb_{50}Ta_{25}$	CoM_2/bcc	33.25	32.00	65.58	28.68
1100	$Co_{80}Nb_5Ta_{15}$	αCo/Co_3M	0.83	2.76	5.70	18.01
	$Co_{80}Nb_{10}Ta_{10}$	αCo/Co_3M	1.58	1.77	11.68	11.99
	$Co_{60}Nb_{10}Ta_{30}$	λ/μ (Co_7M_6)	9.08	23.48	12.89	35.08
	$Co_{60}Nb_{30}Ta_{10}$	λ/μ (Co_7M_6)	24.39	9.02	38.41	10.49
	$Co_{60}Nb_{20}Ta_{20}$	λ/μ (Co_7M_6)	15.42	17.73	26.01	22.20
	$Co_{60}Nb_{35}Ta_5$	λ/μ (Co_7M_6)	29.35	4.38	44.41	5.30
	$Co_{40}Nb_{20}Ta_{40}$	μ (Co_7M_6)/CoM_2	16.41	36.95	18.72	44.76
	$Co_{25}Nb_{10}Ta_{65}$	CoM_2/bcc	6.12	58.76	17.03	80.75
	$Co_{25}Nb_{20}Ta_{55}$	CoM_2/bcc	14.23	50.82	29.77	64.48
	$Co_{25}Nb_{55}Ta_{20}$	CoM_2/bcc	42.28	25.40	77.69	20.13
	$Co_{40}Nb_{50}Ta_{10}$	μ (Co_7M_6)/bcc	42.16	9.86	86.05	9.12
	$Co_{25}Nb_{65}Ta_{10}$	μ (Co_7M_6)/bcc	41.59	10.81	87.97	9.12
	$Co_{25}Nb_{70}Ta_5$	μ (Co_7M_6)/bcc	47.03	5.23	92.21	4.58
1200	$Co_{80}Nb_{10}Ta_{10}$	αCo/Co_3M	2.28	2.50	11.73	11.83
	$Co_{80}Nb_5Ta_{15}$	αCo/Co_3M	1.17	3.87	5.59	18.11
	$Co_{80}Nb_{15}Ta_5$	αCo/Co_3M	3.51	1.17	17.94	5.63
	$Co_{60}Nb_{30}Ta_{10}$	λ/μ (Co_7M_6)	24.44	9.19	35.52	11.45
	$Co_{60}Nb_{35}Ta_5$	λ/μ (Co_7M_6)	29.32	4.38	41.96	5.65
	$Co_{60}Nb_{25}Ta_{15}$	λ/μ (Co_7M_6)	22.81	11.36	32.12	14.16
	$Co_{60}Nb_{20}Ta_{20}$	λ/μ (Co_7M_6)	15.53	17.71	23.81	23.12
	$Co_{60}Nb_{10}Ta_{30}$	λ/μ (Co_7M_6)	9.21	24.11	14.68	31.72
	$Co_{40}Nb_{40}Ta_{20}$	μ (Co_7M_6)/CoM_2	34.76	19.17	39.74	22.65
	$Co_{40}Nb_{20}Ta_{40}$	μ (Co_7M_6)/CoM_2	15.90	40.12	15.81	49.55
	$Co_{25}Nb_{20}Ta_{55}$	CoM_2/bcc	12.84	52.59	25.70	71.49
	$Co_{25}Nb_{10}Ta_{65}$	CoM_2/bcc	6.25	58.77	16.14	80.77
	$Co_{25}Nb_{65}Ta_{10}$	μ (Co_7M_6)/bcc	43.50	9.19	87.60	8.90
	$Co_{40}Nb_{50}Ta_{10}$	μ (Co_7M_6)/bcc	43.25	10.15	86.44	9.23
1300	$Co_{60}Nb_{30}Ta_{10}$	λ/μ (Co_7M_6)	26.14	9.50	38.73	10.94
	$Co_{60}Nb_{25}Ta_{15}$	λ/μ (Co_7M_6)	23.92	11.64	34.72	14.26
	$Co_{60}Nb_{20}Ta_{20}$	λ/μ (Co_7M_6)	16.99	18.51	23.58	22.99
	$Co_{40}Nb_{20}Ta_{40}$	μ (Co_7M_6)/CoM_2	15.62	38.22	18.12	45.80
	$Co_{40}Nb_{50}Ta_{10}$	μ (Co_7M_6)/bcc	44.26	10.03	84.80	10.18
	$Co_{25}Nb_{65}Ta_{10}$	μ (Co_7M_6)/bcc	45.00	9.14	86.86	9.43
	$Co_{25}Nb_{70}Ta_5$	μ (Co_7M_6)/bcc	50.06	4.84	91.66	4.71
	$Co_{25}Nb_{10}Ta_{65}$	CoM_2/bcc	5.90	59.46	18.38	78.74
	$Co_{25}Nb_{20}Ta_{55}$	CoM_2/bcc	13.33	51.62	35.50	61.20

formation behaviors of the analyzed alloy in this study. The small peak at 1406.4 °C means the liquid phase separates out with the temperature increasing, where the μ and bcc phases transform to the liquid phase. The second obvious peak at 1425.7 °C is due to the liquefaction completely. The peak at 1414.8 °C is due to the solidification of the μ phase with the temperature decreasing. The peak at 1391.7 °C corresponds to the eutectic reaction, where the liquid phase transforms to the bcc and μ phases. The transformation temperatures of the Co–Nb–Ta alloys measured by DSC in this work are listed in Table 3, and will be used in the following thermodynamic assessment of the Co–Nb–Ta ternary system.

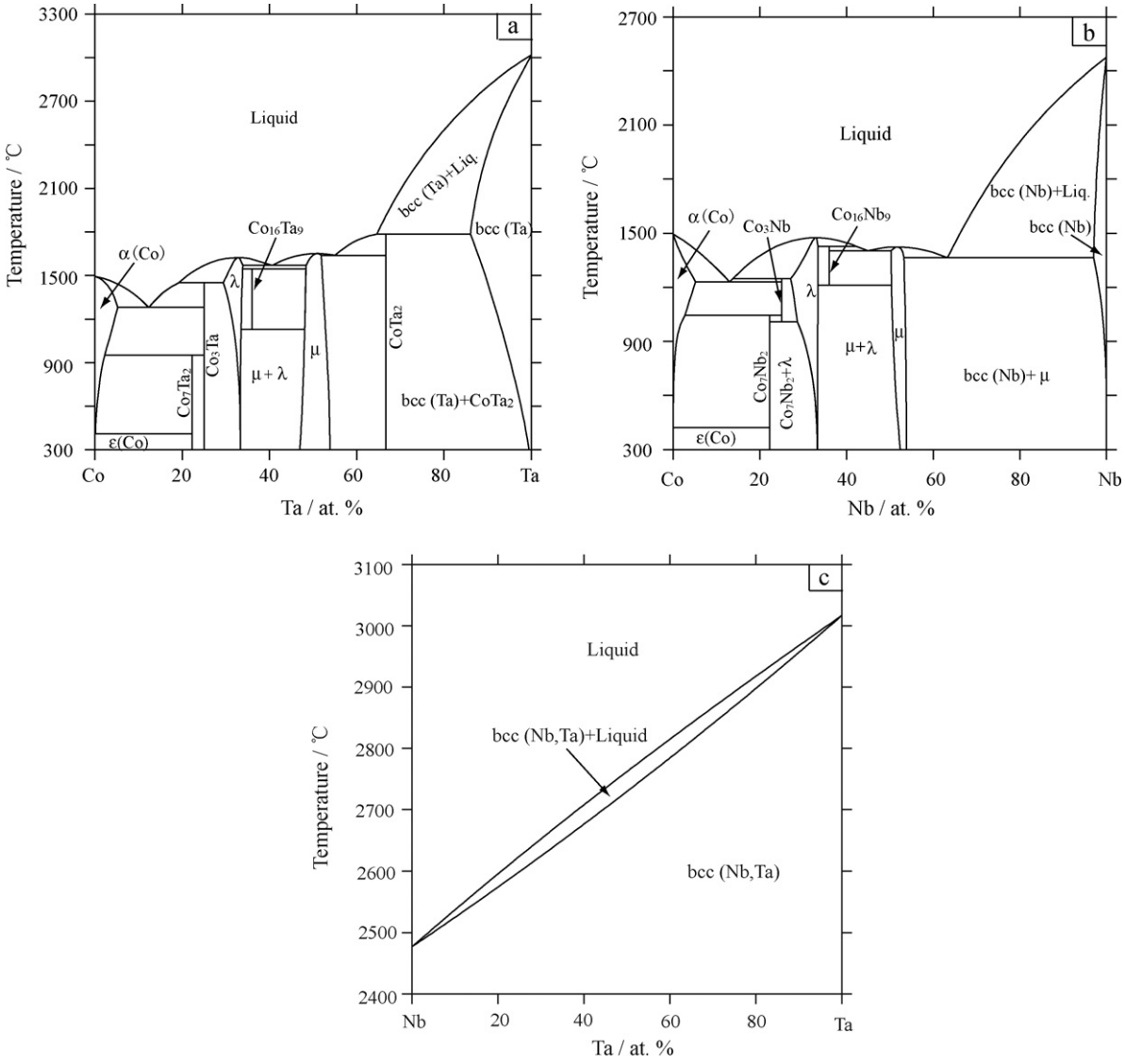

Fig. 4. Calculated binary phase diagrams in the Co–Nb–Ta ternary system: (a) Co–Ta system [15], (b) Co–Nb system [26], and (c) Nb–Ta system [15].

5. Thermodynamic optimization and calculation

5.1. Binary system

The phase diagram of the Co–Ta binary system was thermodynamically assessed by Hari Kumar et al. [15] and Liu [22], respectively, while all the three Laves phases (C14, C15, and C36) generally with an ideal stoichiometry A_2B in Ref. [22] were obviously different from those in experimental phase diagram [23], where the C36 and C14 Laves phases are away from the ideal stoichiometry A_2B, and are nearly stoichiometry Co_3Ta and $Co_{16}Ta_9$, respectively. For this reason, in the present work, the thermodynamic parameters of the Co–Ta binary system reported by Hari Kumar et al. [15] were used. For the Co–Nb binary system, several thermodynamic assessments have been carried out [21,24–26] and the most comprehensive work was performed by Hari Kumar et al. [21], which was employed in this work. The Nb–Ta binary system thermodynamically assessed by Hari Kumar et al. [15] is directly adopted in the present work. The calculated phase diagrams of the Co–Ta, Co–Nb and Nb–Ta systems are shown in Fig. 4(a)–(c), respectively.

Table 3
The transformation temperatures of the Co–Nb–Ta alloys determined by DSC in the present work.

Alloys (at.%)	Transformation temperatures (°C)	
	Heating	Cooling
$Co_{80}Nb_{10}Ta_{10}$	1248.0, 1278.3, 1284.7, 1370.0	1261.1, 1332.0
$Co_{80}Nb_5Ta_{15}$	1013.7, 1291.3, 1413.7,	966.0, 1239.6, 1366.5
$Co_{40}Nb_{50}Ta_{10}$	1406.4, 1425.7	1391.7, 1414.8
$Co_{60}Nb_{35}Ta_5$	1404.4, 1458.7, 1472.4	1395.9, 1435.7, 1457.7

5.2. Ternary system

Because there is no experimental data on the thermodynamic properties of the Co–Nb–Ta system, the ternary thermodynamic parameters were optimized based on the experimental data of the phase equilibria and phase transformation temperatures determined in this work. All the

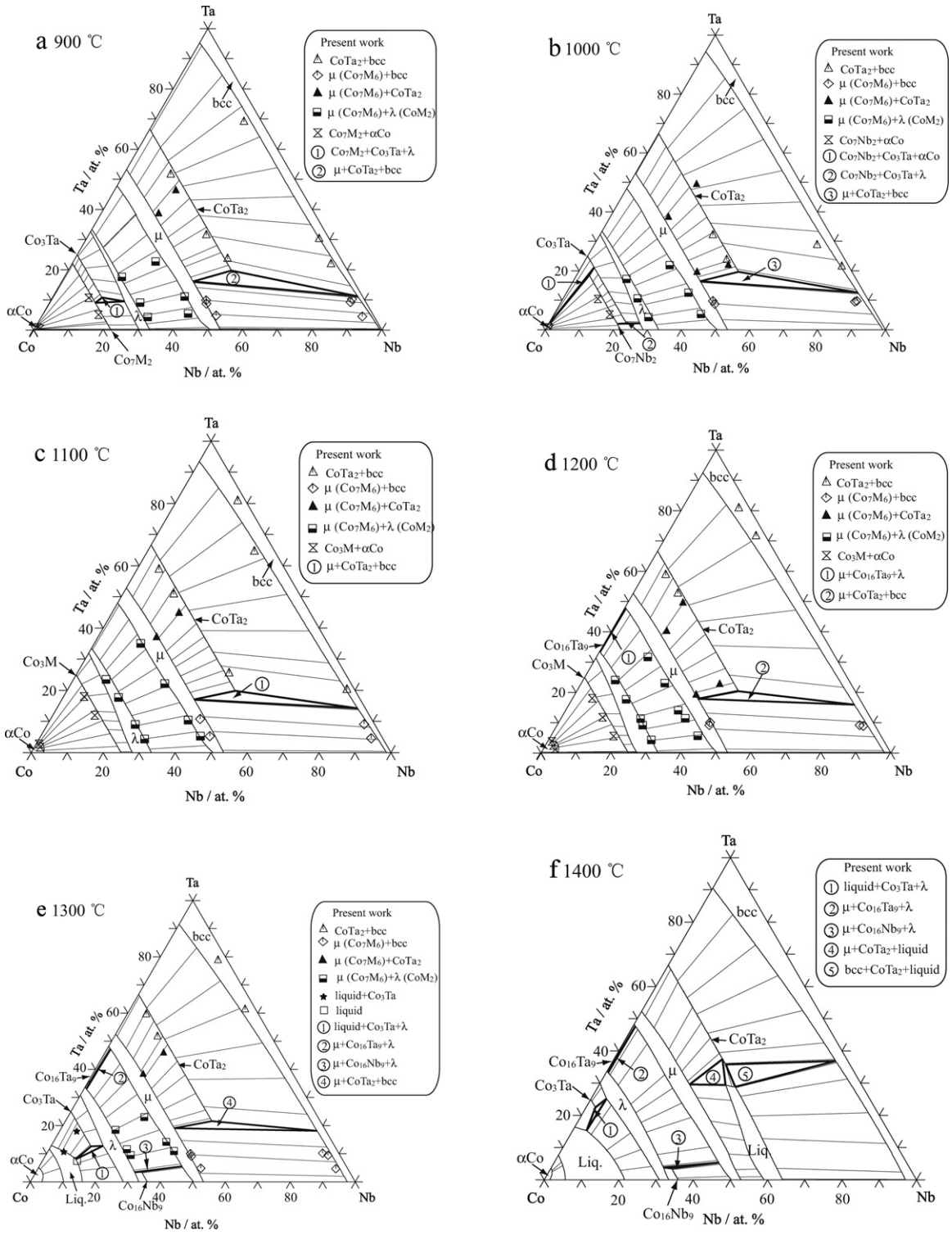

Fig. 5. Calculated isothermal sections of the Co–Nb–Ta ternary system at: (a) 900 °C, (b) 1000 °C, (c) 1100 °C, (d) 1200 °C, (e) 1300 °C, and (f) 1400 °C compared with the experimental data determined in the present work.

thermodynamic parameters optimized in this work are listed in Table 4.

The calculated isothermal sections of the Co–Nb–Ta ternary system at 900 °C, 1000 °C, 1100 °C, 1200 °C, 1300 °C and 1400 °C, compared with the experimental results determined in the present work, are shown in Fig. 5(a)–(f), respectively, where the calculated results are in good agreement with the experimental data marked by different symbols. As can be seen in Fig. 5(a), there is one three-phase region ($\mu + CoTa_2 + bcc$) in the Co–Nb rich side and three continuous single-phase regions (λ, μ and bcc) existing from the Co–Nb side to Co–Ta side, which is the same to the type of phase relationship shown in Fig. 5(b)–(e). The Co_7M_2 phase, a continuous single-phase region from Co–Ta side to Co–Nb side (Fig. 5(a), disappears in the Co–Ta rich side

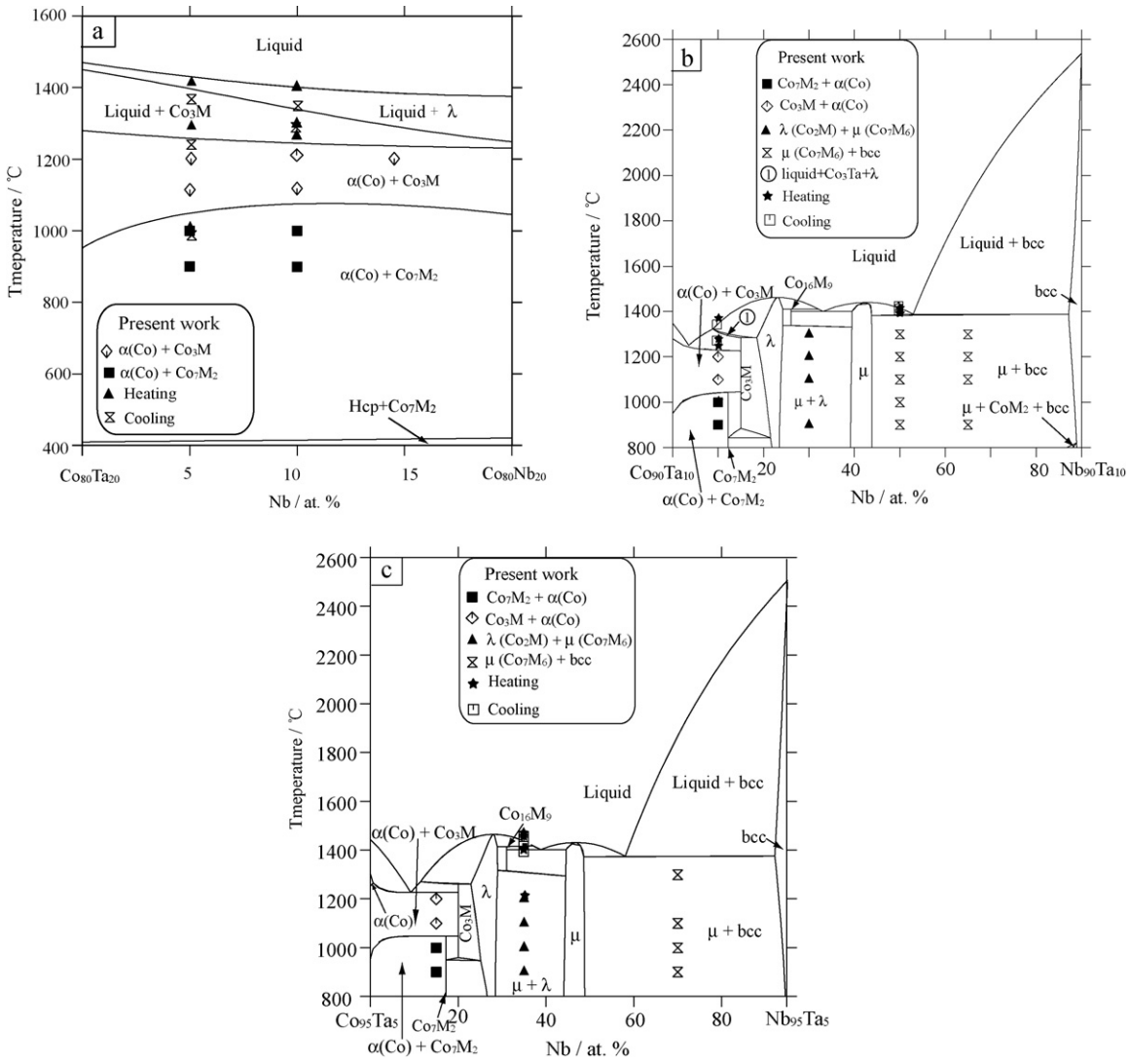

Fig. 6. Calculated vertical sections at: (a) 80 at.% Co, (b) 10 at.% Ta, and (c) 5 at.% Ta in the Co–Nb–Ta system compared with the experimental data determined in the present work.

of the isothermal section at 1000 °C (Fig. 5(b)). Fig. 5(c) presents the calculated isothermal section at 1100 °C, which shows the same phase relationship as that in Fig. 5(d). The liquid phase is in equilibrium with the αCo phase, Co_3Ta phase and λ phase in the isothermal section at 1300 °C (Fig. 5(e)), respectively, and a three-phase region (Liquid + Co_3Ta + λ) also exists in Fig. 5(f). In the isothermal section at 1400 °C shown in Fig. 5(f), two three-phase regions (Liquid + $CoTa_2$ + μ and Liquid + bcc + $CoTa_2$) appear.

The calculated vertical sections of the Co–Nb–Ta system at 80 at.% Co, 10 at.% Ta and 5 at.% Ta compared with the experimental data in the present work are shown in Fig. 6(a)–(c), respectively. The alloys of $Co_{80}Nb_5Ta_{15}$ in Fig. 6(a), $Co_{80}Nb_{10}Ta_{10}$ in Fig. 6(b), $Co_{80}Nb_{15}Ta_5$ in Fig. 6(c) and so on transform with the temperature increasing, and the transformations are observed intuitively in vertical sections. And the calculated results shown in the calculated vertical sections are good agreement with the experimental data. Fig. 7 shows the calculated liquidus projection using the thermodynamic parameters optimized in the present work. As can be obviously seen in Fig. 7, two invariant points exist in the liquidus curve, and details about the calculated invariant reactions are listed in Table 5.

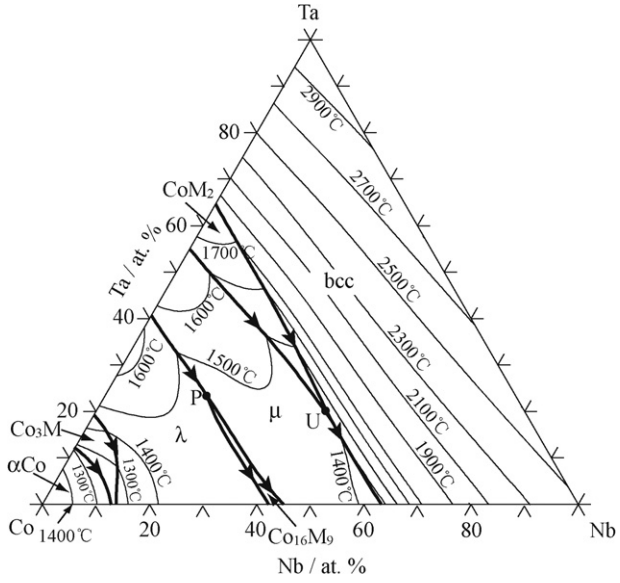

Fig. 7. Calculated liquidus projection in the Co–Nb–Ta ternary system.

Table 4
Thermodynamic parameters of the Co–Nb–Ta ternary system optimized by the present work.

Parameters in each phase (J/mol)
Liquid, format: (Co, Nb, Ta)
${}^{0}L^{\text{Liq.}}_{\text{Co,Nb,Ta}} = -70,000$
${}^{1}L^{\text{Liq.}}_{\text{Co,Nb,Ta}} = 34,000$
${}^{2}L^{\text{Liq.}}_{\text{Co,Nb,Ta}} = 30,000$

Bcc_A2, format: (Co, Nb, Ta)
${}^{0}L^{\text{bcc}}_{\text{Co,Nb,Ta}} = -339,600 + 200 \times T$
${}^{1}L^{\text{bcc}}_{\text{Co,Nb,Ta}} = -481,900 + 300 \times T$
${}^{2}L^{\text{bcc}}_{\text{Co,Nb,Ta}} = -3000$

Fcc_A1 (αCo), format: (Co, Nb, Ta)
${}^{0}L^{\text{fcc}}_{\text{Co,Nb,Ta}} = 155,714 - 220 \times T$
${}^{1}L^{\text{fcc}}_{\text{Co,Nb,Ta}} = -2000$
${}^{2}L^{\text{fcc}}_{\text{Co,Nb,Ta}} = -2000$

Hcp_A3 (εCo), format: (Co, Nb, Ta)
${}^{0}L^{\text{fcc}}_{\text{Co,Nb,Ta}} = 0$

Co_7M_2 phase, format: $(Co)_7(Nb, Ta)_2$
${}^{1}L^{\text{fcc}}_{\text{Co,Nb,Ta}} = -2000$

Co_3M phase, format: $(Co)_3(Nb, Ta)_1$
$G^{\text{Co}_3\text{M}}_{\text{Co:Ta}} = 3 \times {}^{0}G^{\text{SER}}_{\text{Co}} + {}^{0}G^{\text{SER}}_{\text{Ta}} - 108,658 + 16.532 \times T$
${}^{0}L^{\text{Co}_3\text{M}}_{\text{Co:Nb,Ta}} = 2000$

$Co_{16}M_9$ phase, format: $(Co)_{16}(Nb, Ta)_9$
$G^{\text{Co}_{16}\text{M}_9}_{\text{Co:Ta}} = 16 \times {}^{0}G^{\text{SER}}_{\text{Co}} + 9 \times {}^{0}G^{\text{SER}}_{\text{Ta}} - 788,956.74 + 107.826 \times T$
${}^{0}L^{\text{Co}_{16}\text{M}_9}_{\text{Co:Ta}} = 52,341.05 - 38.85 \times T$

μ (Co_7M_6) phase, format: $(Co, Nb, Ta)_1(Co, Nb, Ta)_2(Co)_6(Nb, Ta)_4$
${}^{0}L^{\mu}_{\text{Co,Ta:Nb:Co:Nb}} = -75,000$
${}^{0}L^{\mu}_{\text{Co,Ta:Nb:Co:Nb}} = 500,000$

CoM_2 phase, format: $(Co)_1(Nb, Ta)_2$
${}^{0}L^{\text{CoM}_2}_{\text{Co:Ta}} = -45,734.509 + 28.333 \times T$
$G^{\text{CoM}_2}_{\text{Co:Ta}} = {}^{0}G^{\text{SER}}_{\text{Co}} + 2 \times {}^{0}G^{\text{SER}}_{\text{Ta}} - 65,519 + 3.495 \times T$

Table 5
The calculated invariant reactions of the Co–Nb–Ta ternary system.

Invariant reaction	Type	T (°C)	Liquid composition (at.% Nb)	Liquid composition (at.% Ta)	Reference
$L + \lambda + \mu \rightarrow Co_{16}M_9$	P	1404.13	18.83	23.57	This work
		1542.68	0.42	40.27	[15]
$L + CoM_2 \rightarrow bcc + \mu$	U	1383.75	44.76	18.23	This work
		1352.42	55.67	8.02	[15]

6. Conclusions

The isothermal sections of the Co–Nb–Ta ternary system at 900 °C, 1000 °C, 1100 °C, 1200 °C, and 1300 °C were experimentally determined, and no ternary compound was found in the Co–Nb–Ta ternary system. A consistent set of optimized thermodynamic parameters based on the experimental data have been derived for describing the Gibbs free energies of the solution phases and intermetallic compounds in the Co–Nb–Ta system, which leads good agreement between calculation and most of the experimental data.

Acknowledgements

This work was supported by the National Natural Science Foundation of China (Grant No. 51031003), the Ministry of Education of China (Grant No. 707037) and the Ministry of Science and Technology of China (Grant Nos. 2009DFA52170 and 2009AA03Z101). The Support from Fujian Provincial Department of Science & Technology (Grant No. 2009I0024), Xiamen City Department of Science & Technology (Grant No. 3502Z20093001), and Aviation Science Fund (Grant No. 2009ZF68010) are also acknowledged. We also thank for the support from the Global COE project (Japan).

References

[1] W. Betteridge, Cobalt and Its Alloys, Halsted Press, Chichester, UK, 1982.
[2] S. Iwasaki, K. Quchi, IEEE Trans. Magn. 14 (1978) 849–851.
[3] J. Sato, T. Omori, K. Oikawa, I. Ohnuma, R. Kainuma, K. Ishida, Science 312 (2006) 90–91.
[4] C.T. Sims, W.C. Hagel, The Superalloys, Wiley, New York, 1972, pp. 145–185.
[5] S. Iwasaki, Y. Nakamura, IEEE Trans. Magn. Mag. 13 (1997) 1272–1277.
[6] H. Chinen, doctoral thesis, Tohoku University (2010).
[7] C.P. Wang, J. Wang, X.J. Liu, I. Ohnuma, R. Kainuma, K. Ishida, J. Alloys Compd. 453 (2008) 174–179.
[8] Y. Yu, C.P. Wang, X.J. Liu, I. Ohnuma, R. Kainuma, K. Ishida, Intermetallics 16 (2008) 1199–1205.
[9] C.P. Wang, J. Wang, S.H. Guo, X.J. Liu, I. Ohnuma, R. Kainuma, K. Ishida, Intermetallics 17 (2009) 642–650.
[10] C.P. Wang, P. Yu, X.J. Liu, I. Ohnuma, R. Kainuma, K. Ishida, J. Alloys Compd. 457 (2008) 150–156.
[11] J. Sato, T. Omori, K. Oikawa, K. Ishida, Mater. Trans. 46 (2005) 1199.
[12] T. Omori, Y. Sutou, K. Oikawa, R. Kainuma, K. Ishida, Mater. Sci. Eng. A 438–440 (2006) 1045.
[13] H. Chinen, J. Sato, T. Omori, K. Oikawa, I. Ohnuma, R. Kainuma, K. Ishida, Scripta Mater. 56 (2007) 141–143.
[14] K. Shinagawa, T. Omori, J. Sato, K. Oikawa, I. Ohnuma, R. Kainuma, K. Ishida, Mater. Trans. 49 (6) (2008) 1474–1479.
[15] K.C. Hari Kumar, T. Van Rompaey, P. Wollants, Z. Metallkd. 93 (11) (2002) 1146–1153.
[16] L. Kaufman, H. Bernstein, Computer Calculation of Phase Diagram, Academic Press, New York, 1970.
[17] N. Saunders, A.P. Miodownik, CALPHAD (Calculation of Phase Diagrams)—A Comprehensive Guide, Pergamon Press, 1998.
[18] H. Lukas, S.G. Fries, B. Sundman, Computational Thermodynamics—The CALPHAD Method, Cambridge University Press, 2007.
[19] O. Redlich, A.T. Kister, Ind. Eng. Chem. 40 (1948) 345–348.
[20] M. Hillert, M. Jarl, CALPHAD 2 (1978) 227–238.
[21] K.C. Hari Kumar, I. Ansara, P. Wollants, L. Delaey, J. Alloys Compd. 267 (1998) 105–112.
[22] Z.K. Liu, CALPHAD 23 (1999) 339–356.
[23] E.A. Brandes (Ed.), Smithells Netals Reference Book, Butterworths, Woburn, MA, USA, 1983.
[24] L. Kaufman, H. Nesor, Metall. Trans. 6 (A) (1975) 2115–2122.
[25] L. Kaufman, H. Nesor, CALPHAD 2 (1978) 81.
[26] R. Bormann, R. Busch, J. Non Cryst. Solids 117/118 (1990) 539–542.